Separation and Purification Technology 62 (2008) 423–436

Contents lists available at ScienceDirect

Separation and Purification Technology

journal homepage: www.elsevier.com/locate/seppur

Mechanisms of photocatalytic degradation of Victoria Blue R using nano-TiO_2

F.D. Mai [b], C.S. Lu [a], C.W. Wu [c], C.H. Huang [c], J.Y. Chen [c], C.C. Chen [a,*]

[a] Department of General Education, National Taichung Nursing College, Taichung 403, Taiwan, ROC
[b] Department of Biochemistry, School of Medicine, Taipei Medical University, Taipei 110, Taiwan, ROC
[c] Department of Applied Chemistry, Chung-Shan Medical University, Taichung 402, Taiwan, ROC

ARTICLE INFO

Article history:
Received 30 August 2007
Received in revised form 3 February 2008
Accepted 11 February 2008

Keywords:
Victoria Blue R
Dye
Photocatalytic
Nano-TiO_2
HPLC–PDA–ESI-MS

ABSTRACT

The TiO_2-mediated photocatalysis process was used to successfully degrade dye pollutants. To better understand the mechanistic details of this TiO_2-assisted photodegradation of the Victoria Blue R (VBR) dye with UV irradiation, forty-four intermediates of the process were separated, identified and characterized by HPLC–PDA–ESI-MS (high performance liquid chromatography–photodiode array–electrospray ionization-mass spectrometry) technique in this study, and their evolution during the photocatalytic reaction is presented. The results indicated that the *N*-de-alkylation degradation of VBR dye took place in a stepwise manner to yield mono-, di-, tri-, tetra-, penta-, hexa-*N*-de-methylated and mono-*N*-de-ethylated VBR species, with *N*-hydroxyalkylated intermediates generated during the process. Moreover, the oxidative degradation yielded 4-diethylaminophenol, 4-diethylamino-4′-diethylaminobenzophenone, 4-(*N*,*N*-dimethylaminophenyl)-4′-(*N*′-ethylaminonaphthyl)ketone, 4-(*N*-ethylamino)naphthenol and their *N*-de-alkylated products. The reaction mechanisms of TiO_2/UV proposed in this study should be useful for future application of the technology to the degradation of dyes.

1. Introduction

Triphenylmethane dyes are suitable for a large variety of technological applications. They have been extensively used as textile dyes for silk, wool, and cotton, in the preparation of inks and in the surface-coating and dyeing of paper [1,2], as colorants in foods, drugs, cosmetics [3], as biological stains, and as anti-infective, antimicrobial and antihelmintic agents [1]. The photocytotoxicity of triphenylmethane dyes, based on the production of the reactive oxygen species, is tested intensively with the regard to their photodynamic treatment [4]. Nelson and Hites [5] reported the deposition of Crystal Violet and Malachite Green in the sediment and water of Buffalo River in New York. They found aniline dyes in aquatic environmental. From a study of Black et al. [6], it was shown that aniline dyes could be mutagenic and carcinogenic to biota. An additional worrying factor is that some triphenylmethane dyes have been shown to be potent clastogens, possibly responsible for promoting tumor growth in some species of fish [7–9]. Doerge et al. [10] have demonstrated that leucomalachite green inhibits thyroid peroxidase-catalyzed formation of thyroxine and tyrosine in vitro, which also results in the oxidative *N*-demethylation of leucomalachite green to a primary phenylamine. They suggested that the anti-thyroid effects observed in rats treated with leucomalachite green result from blockage of hormone synthesis through alternate substrate inhibition and that chronic exposure could cause thyroid gland follicular cell tumors through a hormonal mechanism. Moreover, the formation of a primary arylamine, which may be metabolically activated and bind to DNA, raises the possibility of a genotoxic mechanism for tumor formation. However, the thyroid peroxidase-catalyzed oxidation of the triphenylmethane class of dyes has aroused great concern because the reactions might form various *N*-de-alkylated primary and secondary aromatic amines, with structures similar to aromatic amine carcinogens [11–13]. In early report [14], it describe how the molecular structure of four cationic triphenylmethane dyes, VBR, Victoria Pure Blue BO, Crystal Violet, and Ethyl Violet, affects their efficiency as mediators of the photoinduced inactivation of two model mitochondrial targets, hexokinase and DNA. Hexokinase is known to be over-expressed in highly glycolytic tissues such as tumors, and this enzyme has been previously considered as a possible target for anti-tumor therapy. Mitochondrial DNA is particularly prone to oxidative damage due to both its lack of protective histones and proofreading and the presence of incomplete repair mechanisms in the mitochondrial machinery.

The TiO_2-mediated photocatalysis process has been successfully used to degrade pollutants during the past few years [15–17]. TiO_2 is broadly used as a photocatalyst because of its non-toxicity, photochemical stability, and low cost [18]. Heterogeneous photocatalysis is an emerging destructive technology leading to the total mineralization of many dye pollutants through the proposed mechanism [19].

* Corresponding author. Tel.: +886 4 2219 6975; fax: +886 4 2219 4990.
E-mail address: ccchen@mail.ntcnc.edu.tw (C.C. Chen).

1383-5866/$ – see front matter © 2008 Elsevier B.V. All rights reserved.
doi:10.1016/j.seppur.2008.02.006

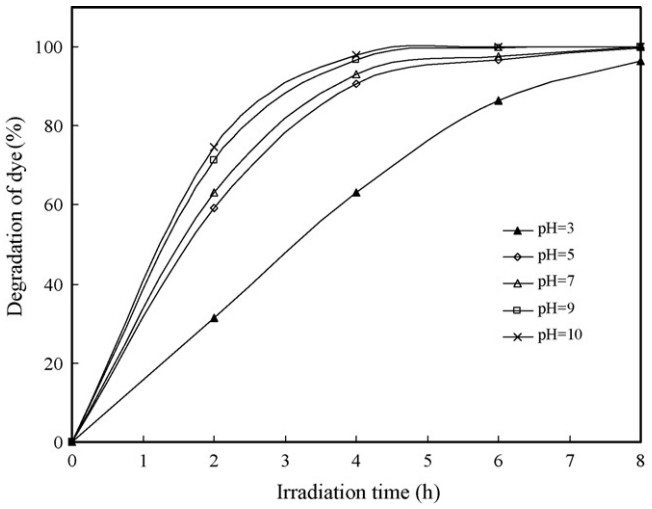

Fig. 1. pH effect on the VBR photodegradation rate with concentrations of TiO_2 to be 0.5 g L^{-1} and VBR to be 0.05 g L^{-1}.

Studies on the photocatalytic degradation of different classes of organics have appeared in the literature, and most of them include a detailed examination of the so-called primary processes under different working conditions [20–22]. However, less attention has been paid to the study of the degradation mechanism and to the identification of major transient intermediates, which have been more recently recognized as very important aspects of these processes, especially in view of their practical applications.

In earlier reports [23–25], the photodegradation of the triphenylmethane dyes were investigated. The *N*-de-alkylation process was predicated on the basis of the wavelength shift of the maximal absorption of the dyes. However, only some of the *N*-de-alkylation intermediates of these dyes have been isolated and identified.

In this paper, we report on the photocatalytic degradation of VBR [bis(4-dimethylaminophenyl) (4-ethylaminonaphthenyl)methylium chloride; Basic Blue 11; C. I. 44040] for the first time. The objectives were to study the photodegradation efficiency and identify the main intermediates in order to determine the degradation mechanism.

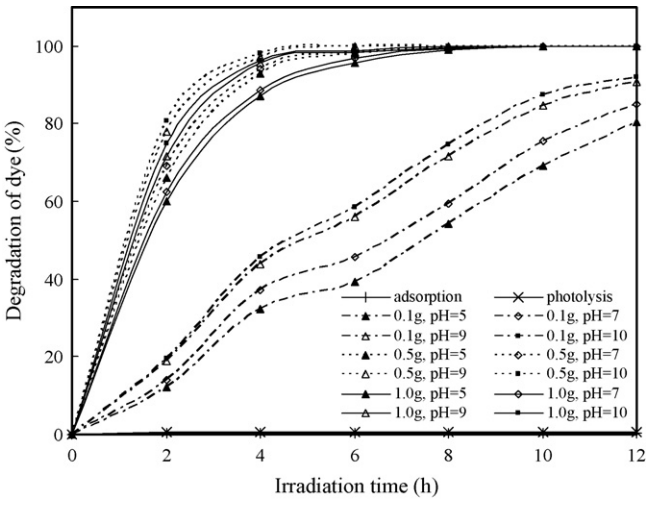

Fig. 2. Influence of the catalyst concentration on the photodegradation efficiency for the decomposition of VBR.

2. Experimental

2.1. Materials

Titanium dioxide (P25)—a known mixture of 80% anatase and 20% rutile form with an average particle size of 30 nm, nonporous, and with a reactive surface area of $50 \pm 10\ m^2\ g^{-1}$—was used as-received for all degradation experiments. VBR dye was obtained from Sigma–Aldrich and used without any further purification. HPLC analysis confirmed the presence of VBR as the only organic compound. 4-(*N*-methylaminophenol) (MAP; with a guaranteed purity of 98%) and 4-amioonaphthen-1-ol (purity of 90%) were obtained from Aldrich. 4-aminophenol (AP; analytical standard) was purchased from Riedel-deHaen. The 4-(*N*,*N*-dimethylamino)-4′-(*N*′,*N*′-dimethylamino)benzophenone was obtained from Acros Organics. Reagent-grade ammonium acetate, sodium hydroxide, nitric acid, and HPLC-grade methanol were purchased from Merck. De-ionized water was used throughout this study. The water was then purified with a Milli-Q water ion-exchange system (Millipore Co.) to give a resistivity of 18 MΩ cm.

2.2. Irradiation procedure

Before being irradiated, the suspensions were stirred in the dark for 30 min to reach adsorption equilibrium with the TiO_2 sur-

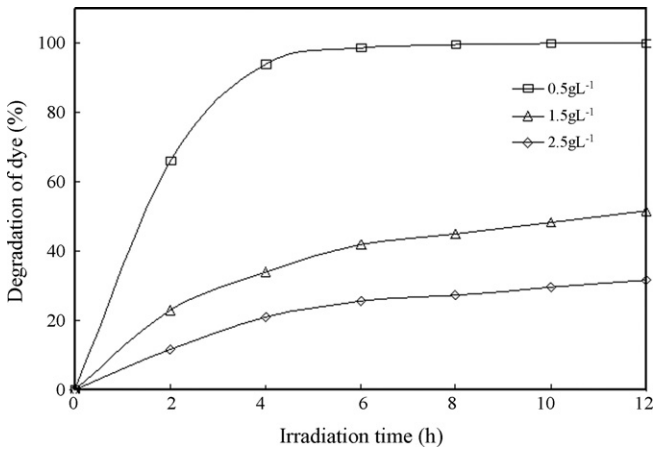

Fig. 3. Influence of initial dye concentration on the photodegradation efficiency for the decomposition of VBR.

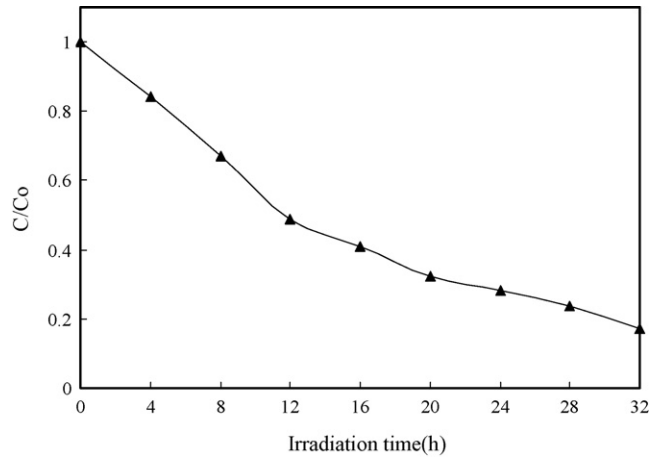

Fig. 4. Depletion in TOC as a function of irradiation time for an aqueous solution of VBR in the presence of TiO_2. Experimental condition: dye concentration (0.05 gL^{-1}), P25 (0.5 gL^{-1}), pH 9, continuous stirring, and irradiation time 32 h.

face. Irradiation experiments of VBR were carried out on stirred aqueous solutions contained in a 100 mL flask. Degradations were performed on 100 mL of aqueous solutions containing the desired concentration of VBR (50 mg L^{-1}) and three different amount of TiO_2 (0.1, 0.5, and 1.0 g L^{-1}) at different pH values. Irradiations were carried out using two UV-365 nm lamps (15 W). At any given irradiation time interval, the dispersion was sampled (5 mL), centrifuged, and subsequently filtered through a Millipore filter (pore size, 0.22 μm) to separate the TiO_2 particles.

Performed in flask without addition of TiO_2, the blank experiments showed no appreciable decolorization of the irradiated solution, and thus confirmed the expected stability of this VBR dye under UV light irradiation. Also with addition of 0.5 g L^{-1} TiO_2 to solutions, which contain 50 mg L^{-1} of the VBR dye, the stability of the dye did not alter in the dark either.

2.3. Instruments and analytical methods

2.3.1. Instruments

A Waters ZQ LC/MS system, equipped with a binary pump, a photodiode array detector, an autosampler, and a micromass detector, was used for separation and identification. The mineral-

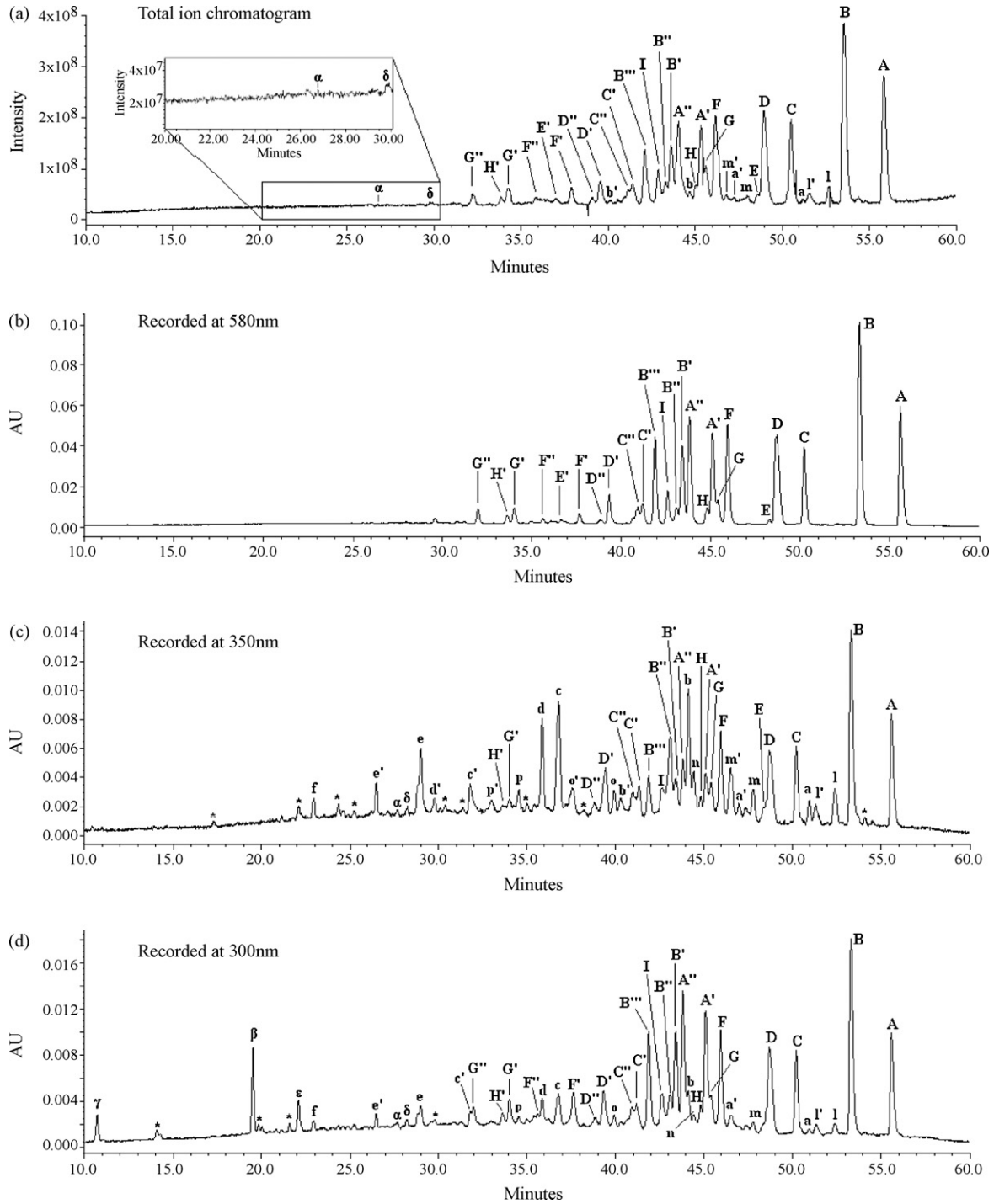

Fig. 5. (a) Total ion chromatogram and HPLC chromatogram of the photocatalytic degradation intermediates with 4 h of irradiation, at pH 9, recorded at (b) 580 nm, (c) 350 nm, (d) 300 nm.

ization of the dye was monitored by measuring the total organic carbon (TOC) content with a Tekmar-Dohrmann Phoenix 8000 TOC Analyzer by directly injecting the aqueous solution. The C-75 Chromato-Vue cabinet of UVP provides a wide area of illumination from the 15-W UV-365 nm tubes (Hitachi) positioned on two sides of the cabinet interior.

2.3.2. Analytical methods

After each irradiation cycle, the amount of the residual dye was thus determined by HPLC. The analysis of organic intermediates was accomplished by HPLC–ESI-MS after a readjustment of the chromatographic conditions to make the mobile phase compatible with the working conditions of the mass spectrometer. Two different kinds of solvents were prepared in this study. Solvent A was 25 mM aqueous ammonium acetate buffer (pH 6.9) while solvent B was methanol instead of ammonium acetate. LC was carried out on an Atlantis^{TM} dC18 column (250 mm × 4.6 mm i.d., dp = 5 μm). The flow rate of the mobile phase was set at 1.0 mL min^{-1}. A linear gradient was set as follows: t = 0, A = 95, B = 5; t = 20, A = 50, B = 50; t = 40–45, A = 10, B = 90; t = 48, A = 95, *B* = 5.

The column effluent was introduced into the ESI source of the mass spectrometer. Equipped with an ESI interface, the quadruple mass spectrometer with heated nebulizer probe at 200 °C was used with an ion source temperature of 120 °C. ESI was carried out with the vaporizer at 200 °C and nitrogen as sheath (551 kPa) and auxiliary (138 kPa) gas to assist with the preliminary nebulization and to initiate the ionization process. A discharge current of 5 μA was applied. Cone lens and capillary voltages were optimized for the maximum response during perfusion of VBR standard.

3. Results and discussion

3.1. pH effect

The zero point charge for TiO_2 is 6.8, and the TiO_2 surface is predominantly negatively charged when the pH is higher than the TiO_2 isoelectric point [26]. As the pH decreases, the functional groups are protonated, and the proportion of the positively charged surface increases. Thus, the electrical property of the TiO_2 surface varies with the pH of the dispersion. The surface of TiO_2 would be negatively charged and adsorb cationic species easily while in the reverse condition it would adsorb anionic ones. However, the adsorption of the substrate onto the TiO_2 surface directly affects the occurrence of electron transfer between the excited dye and TiO_2 and further influences the degradation rate. The surface becomes negatively charged, and the number of adsorption sites may decrease above the isoelectric point of TiO_2. A similar effect of the pH on the adsorption and photocatalytic reaction has been reported for the degradation of methyl green [27].

The photodegradation efficiency of the VBR as a function of reaction pH is shown in Fig. 1. As expected, the rate constant of the VBR dye was found to increase with the increase in pH. Under acidic conditions, it was found difficult to adsorb the cationic VBR dye onto the TiO_2 surface. The active •OH radicals, formed in low concentrations, and hence the photodegradation process of VBR remained slow. With higher pH values, the formation of active •OH species is favored, due to not only improved transfer of holes to the adsorbed hydroxyls, but also electrostatic abstractive effects between the negatively charged TiO_2 particles and the operating cationic dyes. Although the VBR dye can adsorb onto the TiO_2 surface to some extent in alkaline media, when the pH value is too high (pH 11), the VBR dye molecules will change to a leuco-compound. Our results indicate that the TiO_2 surface is negatively charged, and the VBR adsorbs onto the TiO_2 surface through the positive ammonium groups. This is characteristic of heterogeneous photocatalysts, and the results are in agreement with the earlier studies [28].

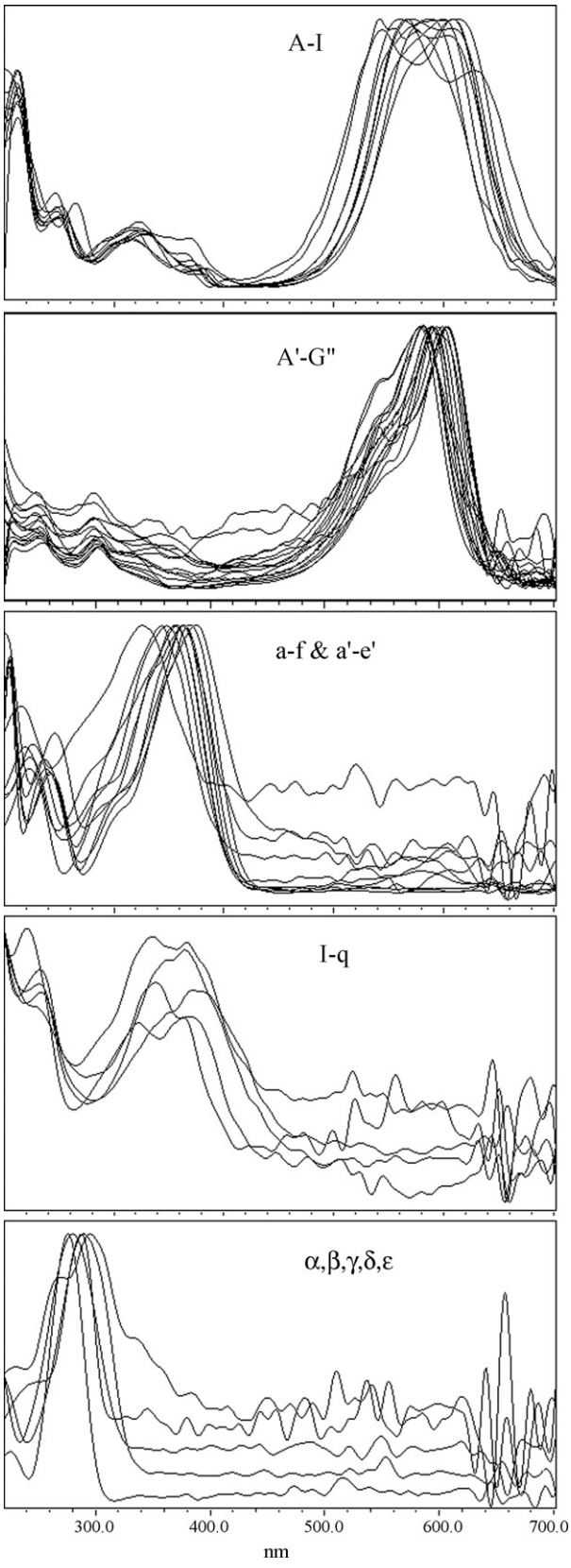

Fig. 6. Absorption spectra of the intermediates formed during the photodegradation process of the VBR dye corresponding to the peaks in the HPLC chromatograph of Fig. 5. Spectra were recorded using the photodiode array detector. Spectra **A**–**I**, **A**′–**G**″, **a**–**f**, **a**′–**e**′, **I**–**q**, and **α**–**ε** correspond to the peaks **A**–**I**, **A**′–**G**″, **a**–**f**, **a**′–**e**′, **I**–**q**, and **α**–**ε** in Fig. 5, respectively.

Table 1
Identification of the *N*-de-alkylation intermediates of the photodecomposed VBR dye by HPLC–PDA–ESI-MS

TIC peaks	Intermediates	$[M+H^+]$	ESI-MS spectrum (m/z) ions	Absorption maximum (nm)
A	Bis(4-dimethylaminophenyl) (4-ethylaminonaphthenyl)methylium	422.30	406.30, 393.25, 378.27, 301.21, 272.15	612.6 582.4
B	(4-dimethylaminophenyl) (4-methylaminophenyl) (4-ethylaminonaphthyl)methylium	408.16	392.10, 379.17, 258.13	607.7 569.7
C	(4-dimethylaminophenyl) (4-aminophenyl) (4-ethylaminonaphthyl)methylium	394.14	365.09, 349.09, 287.13, 258.13	602.8 559.9
D	(4-methylaminophenyl) (4-methylaminophenyl) (4-ethylaminonaphthyl)methylium	394.14	378.14, 349.15, 273.05, 258.01, 229.84	607.7
E	(4-dimethylaminophenyl) (4-dimethylaminophenyl) (4-aminonaphthyl)methylium	394.08	365.15, 349.09, 287.19, 257.94, 223.19	598.6 566.0
F	(4-methylaminophenyl) (4-aminophenyl) (4-ethylaminonaphthyl)methylium	380.13	364.06, 335.32, 273.11, 259.03, 244.12, 229.84	599.1
G	(4-dimethylaminophenyl) (4-methylaminophenyl) (4-aminonaphthyl)methylium	380.32	364.19, 273.11, 259.16, 243.99, 229.84	607.7 544.0
H	(4-aminophenyl) (4-aminophenyl) (4-ethylaminonaphthyl)methylium	366.56	336.60, 273.11, 245.40	588.1
I	(4-dimethylaminophenyl) (4-aminophenyl) (4-aminonaphthyl)methylium	366.24	351.26, 335.13, 259.09, 244.05, 216.91	575.8 541.6
J	(4-methylaminophenyl) (4-methylaminophenyl) (4-aminonaphthyl)methylium	N/A	N/A	N/A
K	(4-methylaminophenyl) (4-aminophenyl) (4-aminonaphthyl)methylium	N/A	N/A	N/A
L	(4-aminophenyl) (4-aminonaphthyl)methylium	N/A	N/A	N/A
A′	(4-hydroxymethylmethylaminophenyl) (4-dimethylmethylaminophenyl) (4-ethylaminonaphthyl)methylium	438.24	409.31, 317.02, 287.96	606.5
A″	Bis(4-dimethylaminophenyl) (4-hydroxyethylaminonaphthyl)methylium	438.18	422.11, 409.12, 317.02, 288.03	602.8
B′	(4-hydroxymethylaminophenyl) (4-methylaminophenyl) (4-ethylaminonaphthyl)methylium	424.10	395.23, 303.07, 275.03	595.4
B″	(4-dimethylaminophenyl) (4-hydroxymethylaminophenyl) (4-ethylaminonaphthyl)methylium	424.48	395.49, 317.47, 288.41	596.7
B‴	(4-dimethylaminophenyl) (4-methylaminophenyl) (4-hydroxyethylaminonaphthyl)methylium	424.16	395.17, 303.19, 273.94, 237.08	593.0
C′	(4-hydroxymethylmethylaminophenyl) (4-aminophenyl) (4-ethylaminonaphthyl)methylium	410.23	381.54, 303.39, 274.58	584.4 546.5
C″	(4-dimethylaminophenyl) (4-aminophenyl) (4-hydroxyethylaminonaphthyl)methylium	410.53	381.54, 317.53, 273.62, 220.43	584.4
D′	(4-hydroxymethylaminophenyl) (4-methylaminophenyl) (4-ethylaminonaphthyl)methylium	410.66	338.33, 301.47	584.4
D″	(4-methylaminophenyl) (4-methylaminophenyl) (4-hydroxyethylaminonaphthyl)methylium	410.21	381.22, 303.26, 274.01	590.5
E′	(4-hydroxymethylaminophenyl) (4-dimethylaminophenyl) (4-aminonaphthyl)methylium	410.14	394.14, 366.11, 323.10, 289.05, 274.07	605.2
F′	(4-hydroxymethylaminophenyl) (4-aminophenyl) (4-ethylaminonaphthyl)methylium	396.25	367.71, 289.43, 214.16	584.4 553.8
F″	(4-methylaminophenyl) (4-aminophenyl) (4-hydroxyethylaminonaphthyl)methylium	396.45	274.46	605.2
G′	(4-hydroxymethylmethylaminophenyl) (4-methylaminophenyl) (4-aminonaphthyl)methylium	396.51	353.50, 303.32, 274.58	607.7
G″	(4-dimethylaminophenyl) (4-hydroxymethylaminophenyl) (4-aminonaphthyl)methylium	396.19	380.06, 288.99	596.7
H′	4-aminophenyl) (4-aminophenyl) (4-hydroxyethylaminonaphthyl)methylium	382.24	260.05, 232.98	594.2
I′	(4-hydroxymethylmethylaminophenyl) (4-aminophenyl) (4-aminonaphthyl)methylium	N/A	N/A	N/A
J′	(4-hydroxymethylaminophenyl) (4-methylaminophenyl) (4-aminonaphthyl)methylium	N/A	N/A	N/A
K′	(4-hydroxymethylaminophenyl) (4-aminophenyl) (4-aminonaphthyl)methylium	N/A	N/A	N/A

3.2. Effect of photocatalyst concentration

It is important from both the mechanistic and application points of view to study the dependence of the photocatalytic reaction rate on the concentration of TiO_2 in the VBR dye. Hence, to investigate the relation between photocatalyst concentration and degradation of dye, the amount of catalyst was varied between 0 and 1 g L^{-1} in a series of experiments under constant process conditions: dye concentration = 50 mg L^{-1}. Fig. 2 shows curves of degraded dye for various catalyst loadings in different pH. As expected, the photodegradation rate of the VBR was found to increase then decrease with the increase in the catalyst concentration, a general characteristic of heterogeneous photocatalyst, and our results are in agreement with the earlier reports [29]. It is known, however, a practical limit of the scattering light exists, above which the degradation rate will decrease due to the reduction of the photonic flux within the irradiated solution.

3.3. Effect of dye concentration

In the typical textile effluent, dye concentration ranges from 0.15 to 0.2 g L^{-1}. By varying the initial concentration from 0.05 to 0.25 g L^{-1} at constant catalyst loading (0.5 g L^{-1}, pH 9), its effect on the degradation rate could be determined, and the results are shown in Fig. 3. As seen in the figure, degradation efficiency is inversely affected by the dye concentration. This negative effect can be explained as follows; as the dye concentration is increased, the adsorption of dye on the catalyst surface active sites increases; hence competitive adsorption of OH^- on the same sites decreases, meaning a lower formation rate of •OH radical, which is the principal oxidant necessary for a high degradation efficiency. On the other hand, considering the Beer–Lambert law, as the initial dye concentration increases, the path length of photons entering the solution decreases, resulting in lower photon absorption on catalyst particles and, consequently, a lower photodegradation rate.

3.4. Evolution of TOC

The complete mineralization of 1 mol VBR dye molecule implies the formation of the equivalent amount (29 mol) of CO_3^{2-} at the end of the treatment. However, the depletion in TOC (shown in Fig. 4) clearly indicates that the reaction does not go to completion. In fact, after 32 h irradiation, about 82.8% of the initial organic carbon has been transformed into CO_2, which implied that there still existed other organic compounds in the irradiated solution. These findings are in agreement with those obtained in a study concerning the photocatalytic degradation of basic violet 4 [30], where the persistence of various aromatic compounds was reported even after long-term irradiation.

3.5. Separation and Identification of the intermediates

Total ion chromatogram obtained for an irradiated VBR solution after 4 h, at pH 9, with UV light in the presence of TiO_2 (0.5 g L^{-1}), and the chromatograms recorded at 580, 350, and 300 nm are illustrated in Fig. 5. With irradiation up to 4 h, forty-four components are identified, all with the retention time less than 60 min. We denoted the VBR dye and its related intermediates as species **A**–**I**, **A′**–**G′′**, **a**–**f**, **a′**–**e′**, **I**–**p**, **I′**–**p′**, **α**–**β**, and **δ**–**ε**. The maximum absorption band of each intermediate in the visible and ultraviolet spectral region in Fig. 6 and Tables 1–2 are measured corresponding to the peaks in Fig. 5, respectively. The intermediates were further identified using the HPLC-ESI mass spectrometric method; the relevant mass spectra are illustrated in Fig. 7 and Tables 1–2. The molecular ion peaks appeared to be in the acid forms of the intermediates. The concentration of the other intermediates may be under the detection limit. From these results, intermediates can be classified to several families:

(1) The first and second families were signed in the chromatogram and are illustrated in Fig. 5b, recorded at 580 nm. From the results of mass spectral analysis, we confirmed that the compo-

Table 2
Identification of the oxidative intermediates of the photodecomposed VBR dye by HPLC–PDA–ESI-MS

HPLC peaks	Intermediates	[M+H$^+$]	Absorption maximum (nm)
a	4-(*N*,*N*-dimethylamino)-4′-(*N*′,*N*′-dimethylamino)benzophenone	269.35	369.1
b	4-(*N*,*N*-dimethylamino)-4′-(*N*′-methylamino)benzophenone	255.64	366.7
c	4-(*N*-methylamino)-4′-(*N*′-methylamino)benzophenone	N/A	363.1
d	4-(*N*,*N*-dimethylamino)-4′-aminobenzophenone	N/A	365.5
e	4-(*N*-methylamino)-4′-aminobenzophenone	N/A	358.1
f	4,4′-bis-aminobenzophenone	N/A	338.2
a′	4-(*N*,*N*-dimethylamino)-4′-(*N*′-hydroxymethyl-*N*′-methylamino)benzophenone	285.43	375.2
b′	4-(*N*-hydroxymethyl-*N*-methylamino)-4′-(*N*′-methylamino)benzophenone	271.78	369.2
b′′	4-(*N*,*N*-dimethylamino)-4′-(*N*′-hydroxymethylamino)benzophenone	N/A	N/A
c′	4-(*N*-methylamino)-4′-(*N*′-hydroxymethylamino)benzophenone	N/A	364.3
d′	4-(*N*-hydroxymethyl-*N*-methylamino)-4′-aminobenzophenone	N/A	363.1
e′	4-(*N*-hydroxymethylamino)-4′-aminobenzophenone	N/A	357.2
I	4-(*N*,*N*-dimethylaminophenyl)-4′-(*N*′-ethylaminonaphthyl)ketone	319.58	367.9
m	4-(*N*-methylaminophenyl)-4′-(*N*′-ethylaminonaphthyl)ketone	305.31	352.6
n	4-(aminophenyl)-4′-(*N*′-ethylaminonaphthyl)ketone	N/A	344.2
o	4-(*N*,*N*-dimethylaminophenyl)-4′-(aminonaphthyl)ketone	N/A	344.5
p	4-(*N*-methylaminophenyl)-4′-(aminonaphthyl)ketone	N/A	340.6
q	4-(aminophenyl)-4′-(aminonaphthyl)ketone	N/A	331.0
I′	4-(*N*-hydroxymethyl-*N*-methylaminophenyl)-4′-(*N*′-ethylaminonaphthyl)ketone	335.61	373.5
I′′	4-(*N*,*N*-dimethylaminophenyl)-4′-(*N*′-hydroxyethylaminonaphthyl)ketone	N/A	N/A
m′	4-(*N*-hydroxymethylaminophenyl)-4′-(*N*′-ethylaminonaphthyl)ketone	321.18	365.5
m′′	4-(*N*-methylaminophenyl)-4′-(*N*′-hydroxyethylaminonaphthyl)ketone	N/A	N/A
n′	4-(aminophenyl)-4′-(*N*′-hydroxyethylaminonaphthyl)ketone	N/A	N/A
o′	4-(*N*-hydroxymethyl-*N*-methylaminophenyl)-4′-(aminonaphthyl)ketone	N/A	356.3
p′	4-(*N*-hydroxymethylaminophenyl)-4′-(aminonaphthyl)ketone	N/A	348.6
α	4-(*N*,*N*-dimethylamino)phenol	138.01	295.2
β	4-(*N*-methylamino)phenol	N/A	290.4
γ	4-aminophenol	N/A	279.7
δ	4-(*N*-ethylamino)naphthenol	188.27	288.1
ε	4-(amino)naphthenol	N/A	276.2

nent **A**, $m/z = 422.30$, in liquid chromatogram is VBR; the other components are **B**, $m/z = 408.16$; **C**, $m/z = 394.14$; **D**, $m/z = 394.14$; **E**, $m/z = 394.08$; **F**, $m/z = 380.13$; **G**, $m/z = 380.32$; **H**, $m/z = 366.56$; **I**, $m/z = 366.24$. The intermediate has the wavelength position of its major absorption band moved toward the blue region, λ_{max}, **A**, 612.6 nm; **B**, 607.7 nm; **C**, 602.8 nm; **D**, 607.7 nm; **E**, 598.6 nm; **F**, 599.1 nm; **G**, 607.7 nm; **H**, 588.1 nm; **I**, 575.8 nm. The first family intermediates may be the *N*-de-alkylation of the VBR dye.From the results of mass spectral analysis, we confirmed that the components are **A′**, $m/z = 438.24$; **A″**, $m/z = 438.18$; **B′**, $m/z = 424.10$; **B″**, $m/z = 424.48$; **B‴**, $m/z = 424.16$; **C′**, $m/z = 410.23$; **C″**, $m/z = 410.53$; **D′**, $m/z = 410.66$; **D″**, $m/z = 410.21$; **E′**, $m/z = 410.14$; **F′**, $m/z = 396.25$; **F″**, $m/z = 396.45$; **G′**, $m/z = 396.51$; **G″**, $m/z = 396.19$; **H′**, $m/z = 382.24$. The *N*-hydroxyalkylated intermediates (the second family), formed by the hydroxylation of the first family, have the wavelength

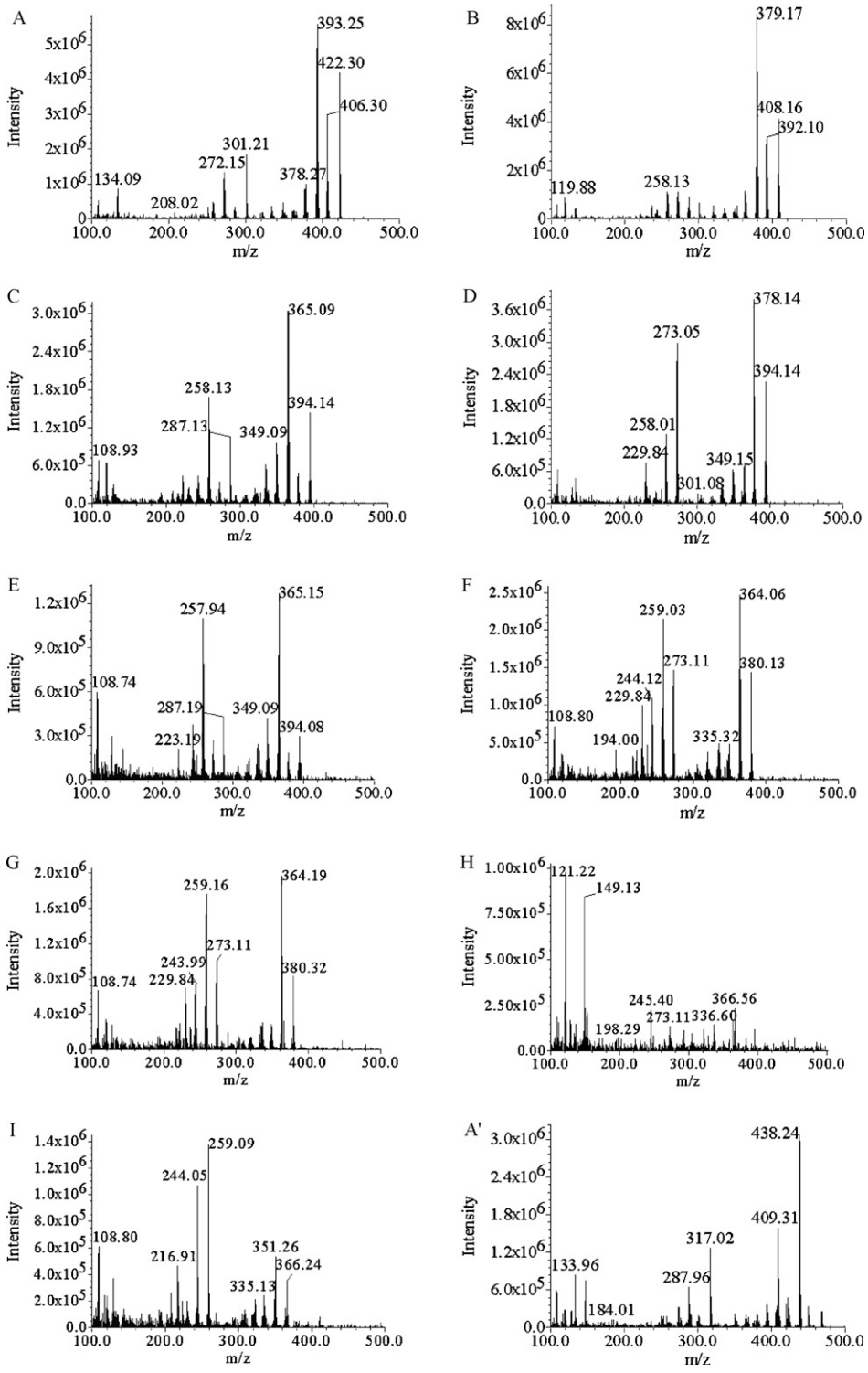

Fig. 7. ESI mass spectra of the intermediates formed during the photodegradation of the VBR dye after they were separated by HPLC method: mass spectra denoted **A**–**I** and **A′**–**G″** correspond to the **A**–**I** and **A′**–**G″** species in Fig. 5, respectively.

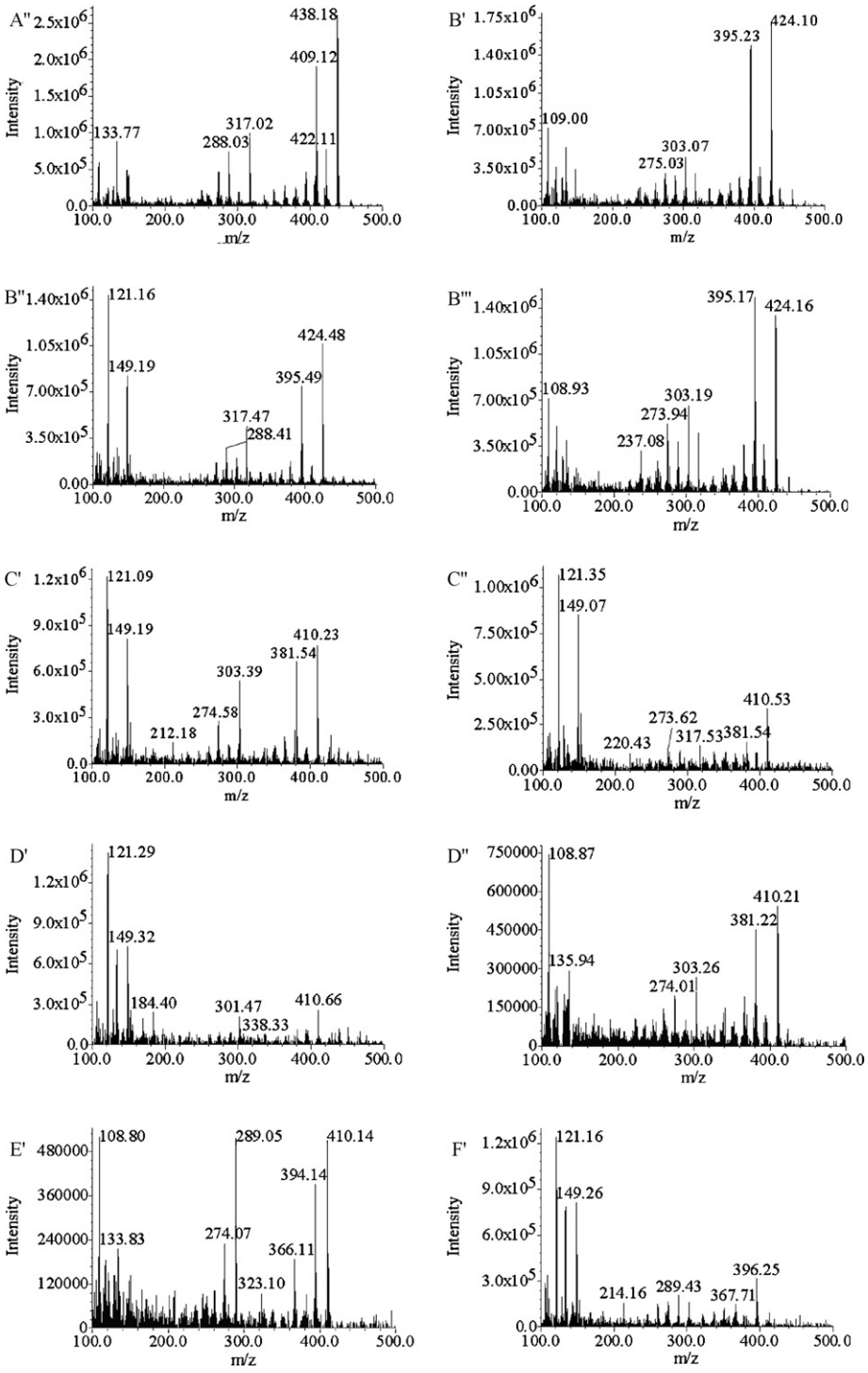

Fig. 7. (*Continued*)

position of their major absorption band, λ_{max}, **A**′, 606.5 nm; **A**″, 602.8 nm; **B**′, 595.4 nm; **B**″, 596.7 nm; **B**‴, 593.0 nm; **C**′, 584.4 nm; **C**″, 584.4 nm; **D**′, 584.4 nm; **D**′, 584.4 nm; **D**″, 590.5 nm; **E**′, 605.2 nm; **F**′, 584.4 nm.; **F**″, 605.2 nm; **G**′, 607.7 nm; **G**″, 596.7 nm; **H**′, 594.2 nm.

(2) The third and fourth families were marked in the chromatogram and are illustrated in Fig. 5c, recorded at 350 nm. From the results of mass spectral analysis, we confirmed that the components are **a**, m/z = 269.35; **b**, m/z = 255.64; **a**′, m/z = 285.43; **b**′, m/z = 271.78. The concentration of the other intermediates may be under the detection limit. The maximum absorption band of each intermediates in the ultraviolet spectral region around 350 nm are displayed in Table 2 corresponding to the peaks **a**–**f** and **a**′–**e**′ in Fig. 5c. The **a**–**f** intermediates, produced by cleavage of the VBR derivatives of the chromophore ring structure or the *N*-de-ethylated **a** in a stepwise manner, has the wavelength position of its major absorption band moved toward the blue region, λ_{max}, **a**, 369.1 nm; **b**, 366.7 nm; **c**, 363.1 nm; **d**, 365.5 nm; **e**, 358.1 nm; **f**, 338.2 nm. The intermediates identified in this study, **a**–**f**, were also identified in a previous study

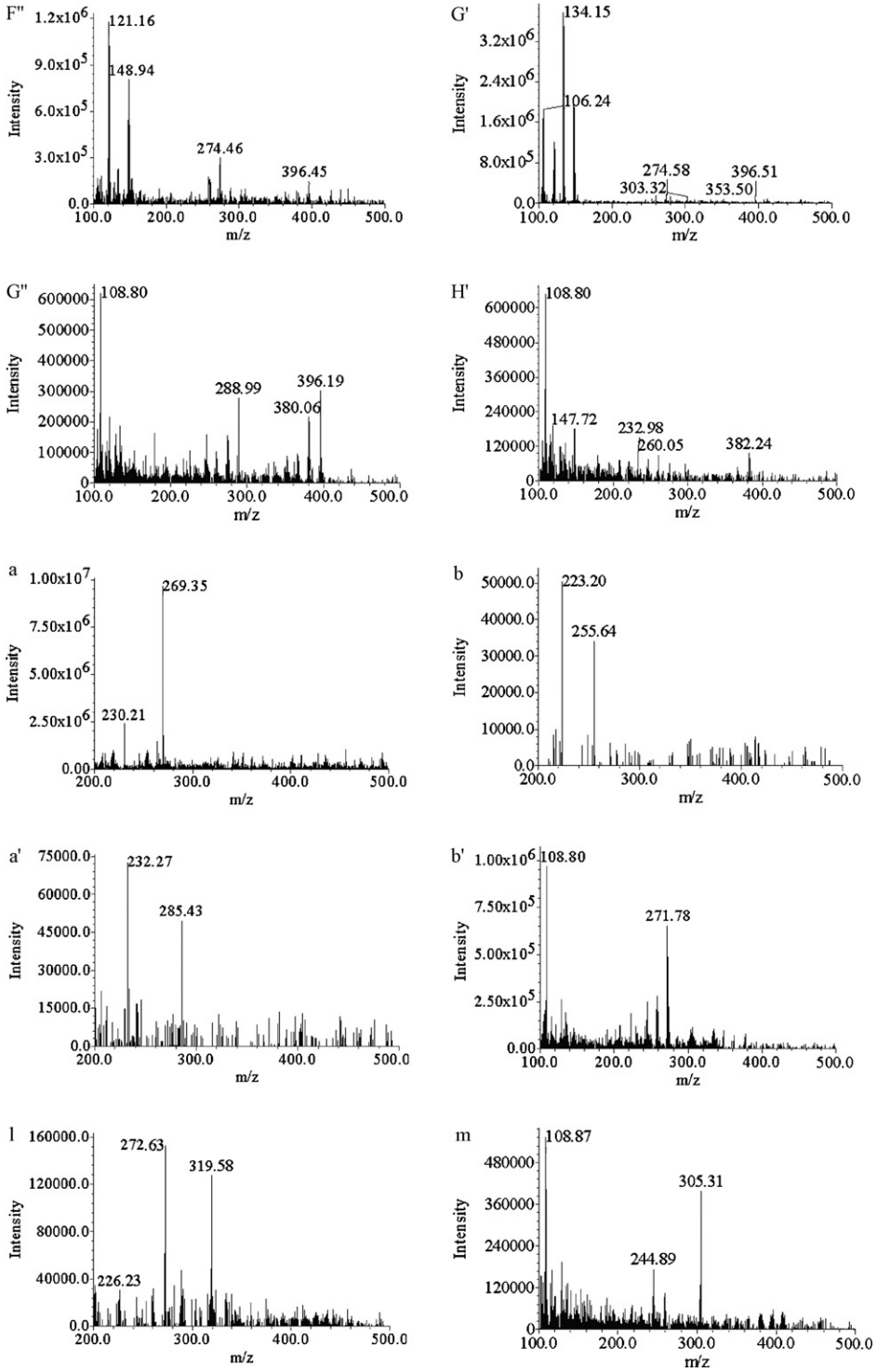

Fig. 7. (*Continued*)

of the MG/TiO_2 system [27]. The hydroxylated intermediates (the fourth family, **a**′–**e**′), produced by the hydroxylation of **a**–**e** intermediates (the third family) or cleavage of the chromophore ring structure of **A**′–**G**″ (the second family), has the wavelength position of its major absorption band moved toward the blue region, λ_{max}, **a**′, 375.2 nm; **b**′, 369.2 nm; **c**′, 364.3 nm; **d**′, 363.1 nm; **e**′, 357.2 nm. The proposed intermediate (**a**) has been compared with standard material of 4-(*N*,*N*-dimethylamino)-4′-(*N*′,*N*′-dimethylamino)benzophenone. The retention times and absorption spectra are identical.

(3) The fifth and sixth families were signed in the chromatogram and are illustrated in Fig. 5c, recorded at 350 nm. From the results of mass spectral analysis, we confirmed that the components are **l**, m/z = 319.58; **m**, m/z = 305.31; **l**′, m/z = 335.61; **m**′, m/z = 321.18. The concentration of the other intermediates may be under the detection limit. The maximum absorption band of each intermediate in the ultraviolet spectral region around 350 nm is showed in Table 2 corresponding to the peaks **l**–**q** and **l**′–**p**′ in Fig. 5c. The **l**–**q** intermediates, produced by cleavage of the chromophore ring structure of **A**–**I** interme-

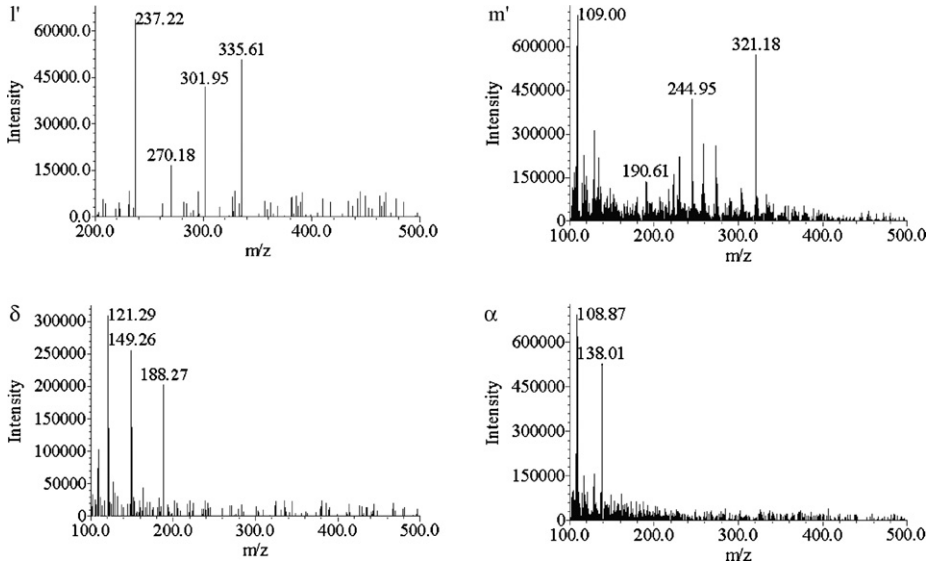

Fig. 7. (*Continued*).

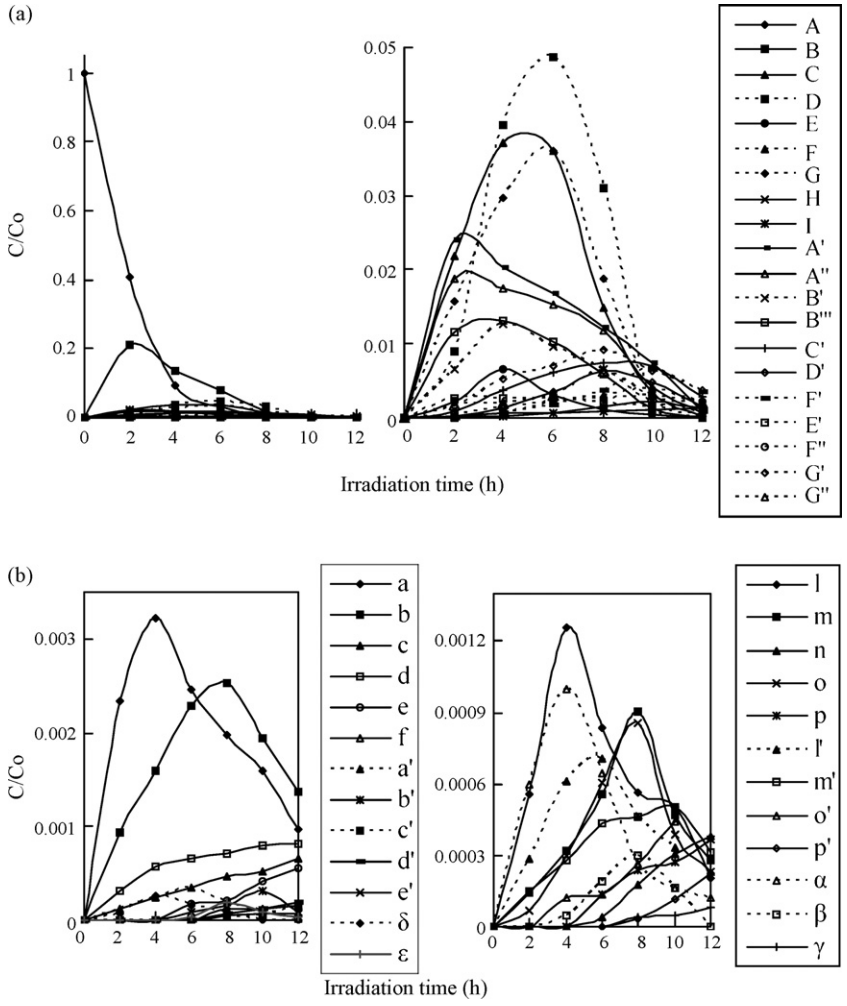

Fig. 8. Variation in the relative distribution of the intermediates obtained from the photodegradation of the VBR dye as a function of the irradiation time. (a) Curves **A–I** and **A′–G″** correspond to peaks **A–I** and **A′–G″** in Fig. 5, respectively. (b) Curves **a–f**, **a′–e′**, **l–p**, and **l′–p′** correspond to peaks **a–f**, **a′–e′**, **l–p**, and **l′–p′** in Fig. 5, respectively.

diates (the first family), has the wavelength position of its major absorption band moved toward the blue region, λ_{max}, **l**, 367.9 nm; **m**, 352.6 nm; **n**, 344.2 nm; **o**, 344.5 nm; **p**, 340.6 nm; **q**, 331.0 nm. The **l′**–**p′** intermediates, produced by cleavage of the chromophore ring structure of **A′**–**G′′** (the second family) or hydroxylation of **l**–**p** intermediates (the fifth family), has the wavelength position of its major absorption band moved toward the blue region, λ_{max}, **l′**, 373.5 nm; **m′**, 365.5 nm; **o′**, 356.3 nm; **p′**, 348.6 nm.

The seventh and eighth families were marked in the chromatogram and are illustrated in Fig. 5d, recorded at 300 nm. From the results of mass spectral analysis, we confirmed that the components are **α**, m/z = 138.01; **δ**, m/z = 188.27. The concentration of the other intermediates may be under the detection limit. The maximum absorption band of each intermediate in the ultraviolet spectral region around 300 nm are showed in Table 2 corresponding to the peaks **α**–**γ** and **δ**–**ε** in Fig. 5d. The two families intermediates, produced by cleavage of the first family's intermediates, has the wavelength position of its major absorption band moved toward the blue region, λ_{max}, **α**, 295.2 nm; **β**, 290.4 nm; **γ**, 279.7 nm; **δ**, 288.1 nm; **ε**, 276.2 nm. The intermediates identified in this study, **α**–**γ**, were also identified in a previous study of the MG/TiO_2 system [27]. The proposed intermediates (**β**, **γ**, **ε**) have been compared with standard materials of 4-(*N*-dimethylamino)phenol, 4-aminophenol, and 4-aminonaphthen-1-ol. The retention times and absorption spectra are identical. The results we observed above can be seen more clearly in Tables 1–2.

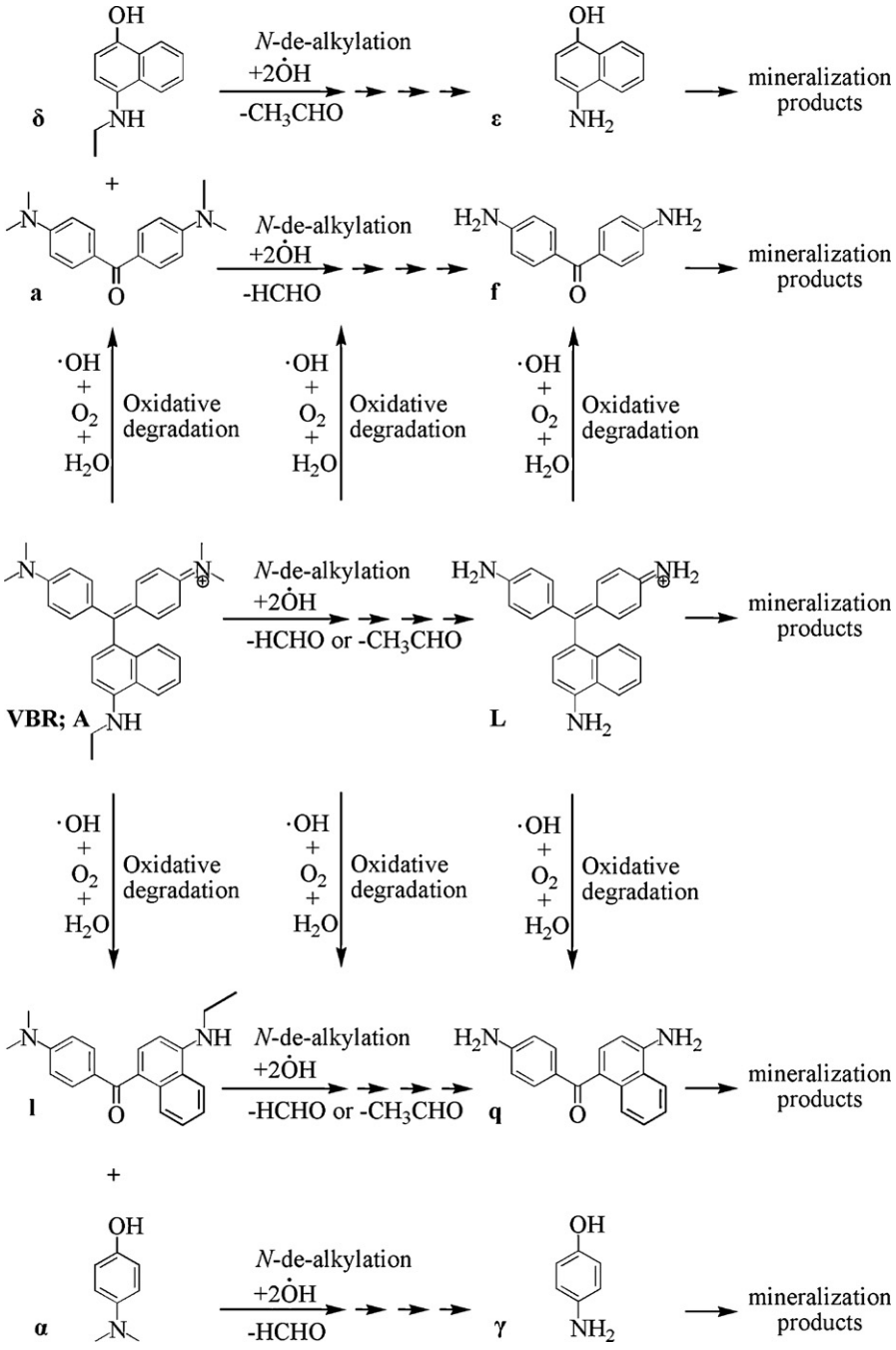

Scheme 1. Proposed mechanisms based on identification of intermediates formed chronologically during the photodegradation of VBR dye by HPLC–ESI-MS.

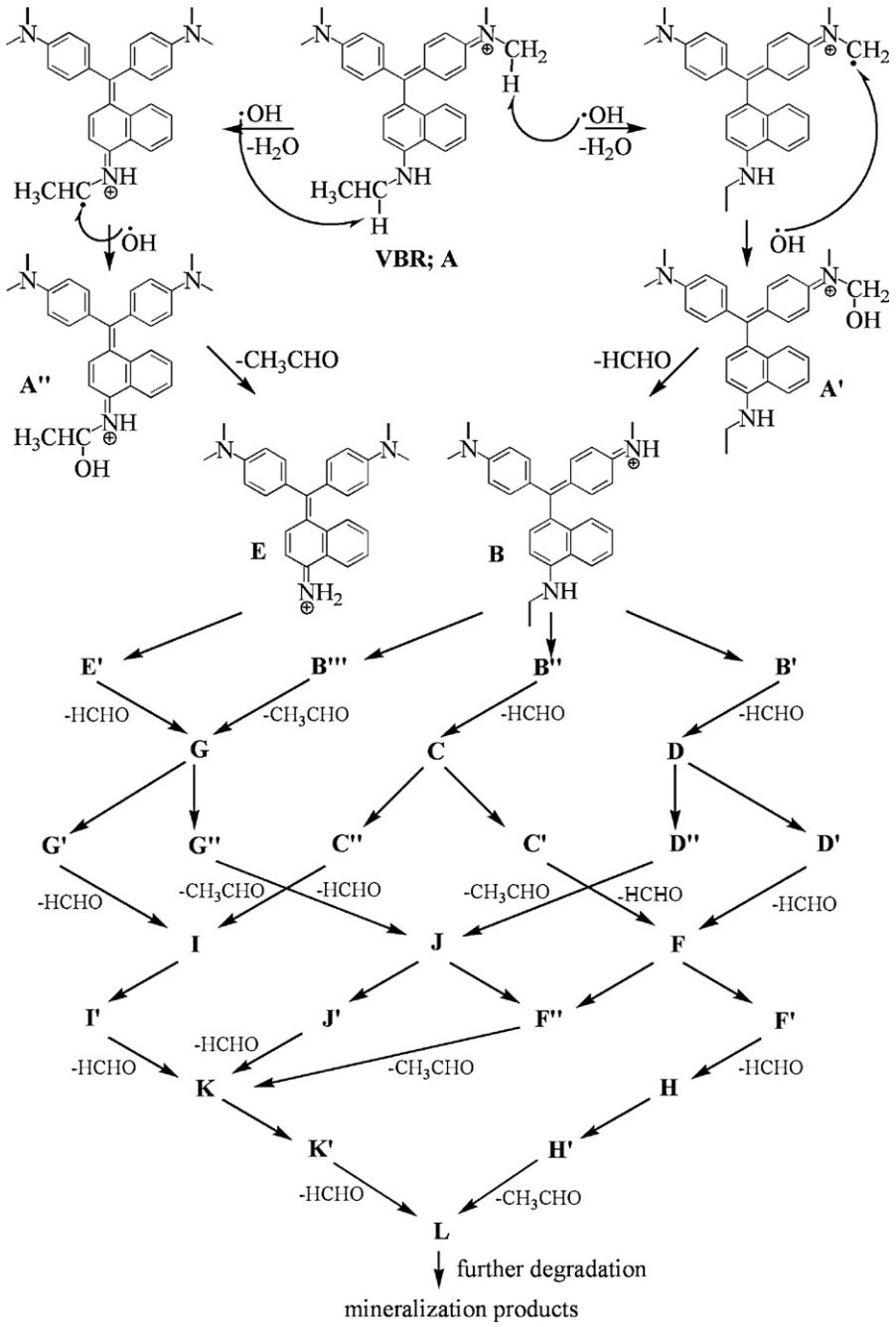

Scheme 2. Proposed *N*-de-alkylation mechanisms based on identification of intermediates formed chronologically during the photodegradation of VBR dye by HPLC–ESI-MS.

3.6. Degradation mechanisms of VBR

On the basis of all the above experimental results, we tentatively propose the mechanism of degradation depicted in Scheme 1. During the initial period of VBR dye photodegradation, competitive reactions between *N*-de-alkylation and oxidative degradation (cleavage of the VBR chromophore ring structure) occurs by the identification of intermediates. The detailed mechanisms are illustrated in the following description.

3.6.1. N-de-alkylation of VBR

The relative distribution of all of the intermediates obtained is illustrated in Fig. 8a. The distributions of all of the *N*-de-alkylated and their hydroxylated intermediates are relative to the initial concentration of VBR. Nonetheless, we clearly observed the changes in the distribution of each intermediate during the photodegradation of VBR. Except for the initial VBR dye (peak **A**), the intensities of the peaks increased at first and subsequently decreased, indicating the formation and transformation of the intermediates. The successive appearance of the maximum of each intermediate indicates that the *N*-de-alkylation of VBR is a stepwise photochemical process by hydroxylated intermediates.

The *N*-de-alkylation of the VBR occurs mostly through attack by the •OH species on the *N*,*N*-dimethyl group or *N*-ethyl group of VBR. In the hydroxylation of VBR, **A**′ or **A**″ reaches its maximum concentration after a 2-h irradiation period because of the •OH attack on the *N*,*N*-dimethyl group or *N*-ethyl group of VBR (curve **A**′ or **A**″). The *N*-mono-de-methylated intermediate, **B**, or the *N*-mono-de-ethylated intermediate, **E**, was clearly observed

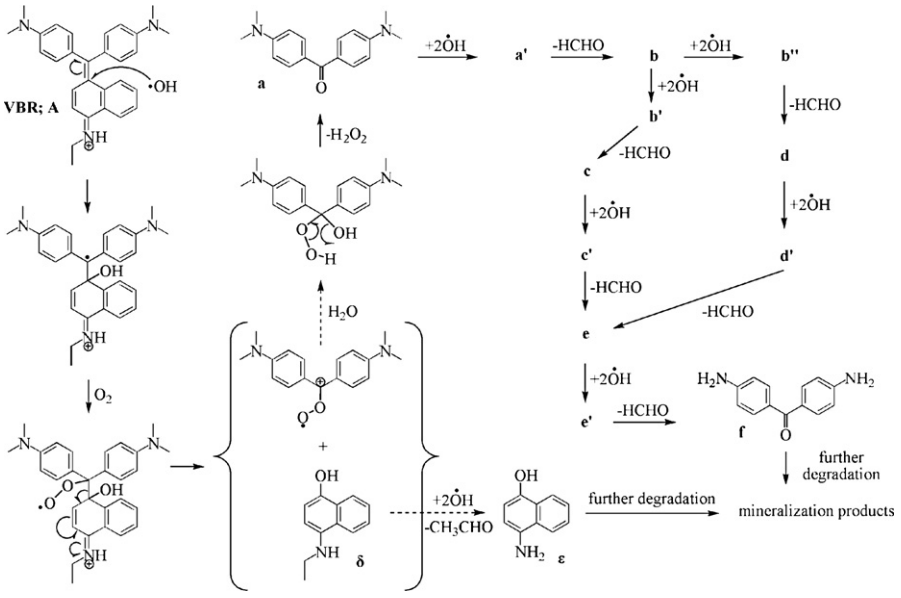

Scheme 3. Proposed mechanism of oxidative degradation of the VBR dye following the identification of intermediates by HPLC–ESI mass spectral techniques.

to reach its maximum concentration after a 2- or 4-h irradiation period (curve **B** or **E**), respectively. The other hydroxylated intermediates, **B′**–**G′**, were clearly observed (curve **B′**–**G″**) to reach their maximum concentration after a 4–10 h irradiation period. The other *N*-alkylated intermediates, **C**–**I**, were clearly observed (curve **C**–**I**) to reach their maximum concentration after a 4–12 h irradiation period. The concentrations of the other *N*-de-alkylated intermediates and hydroxylated intermediates may be too low to be examined by HPLC–PDA–ESI-MS (high performance liquid chromatography–photodiode array–electrospray ionization-mass spectrometry).

The successive appearance of the maximal quantity of each intermediate indicates that the *N*-de-ethylation of VBR is a stepwise photochemical process by the hydroxylated intermediates. VBR gets near the negatively charged TiO_2 particle surface via the positive dimethylamine or ethylamine group. The results discussed above can be seen more clearly from Scheme 2.

3.6.2. Oxidative degradation of the VBR

The oxidative degradation of the VBR dye occurs mostly through attack by the •OH species on the central carbon portion of VBR and produces two sets of intermediates, **a** and **δ** intermediates, and **l** and **α** intermediates. The evolutions of the initial dye concentration and of the identified intermediates were followed as a function of irradiation time. The result is displayed in Fig. 8b. The oxidative degradation of intermediates in the first set were clearly observed (curve **a** and **δ**) to reach their maximum concentrations at the same time after a 4-h irradiation period. In the hydroxylation of an intermediate, **a′** intermediate reached its maximum concentration after a 6-h irradiation period because of the •OH attack on the central carbon of VBR (curve **a′**). The other oxidative intermediates were clearly observed (curve **b**–**f** and **ε**) to reach their maximum concentration after an 8–12-h irradiation period. The other hydroxylated intermediates, **b′**–**e′**, were clearly observed (curve **b′**–**e′**) to reach their maximum concentration after a 10–12-h irradiation period.

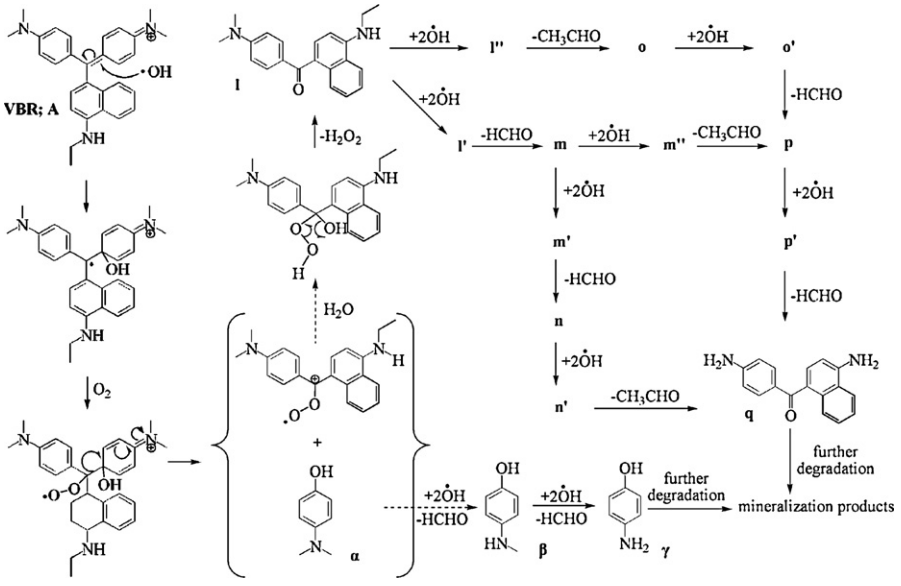

Scheme 4. Proposed mechanism of the oxidative degradation of VBR following the identification of intermediates by HPLC–ESI-MS.

The concentration of the other oxidative intermediates may be under the detectable limit. The results we discussed above can be seen more clearly from Scheme 3.

The second set of intermediates were clearly observed (curve **l** and **α**) to reach their maximum concentrations at the same time after a 4-h irradiation period. In the hydroxylation of **l** intermediate, **l′** and **l″** intermediates reached their maximum concentration after a 6-h irradiation period because of the •OH attack on the central carbon of VBR (curve **l′** and **l″**). The other intermediates were clearly observed (curve **m**–**p** and **β**–**γ**) to reach its maximum concentration after an 8–12-h irradiation period, respectively. The other hydroxylated intermediates, **m′**–**p′**, were clearly observed (curve **m′**–**p′**) to reach their maximum concentration after an 8–12 h irradiation period. The concentration of the other intermediates may be under the detectable limit. The results we discussed above can be seen more clearly from Scheme 4.

According to earlier reports [11,31–33], the *N*-de-alkylation processes are preceded by the formation of a nitrogen-centered radical while oxidative degradation (destruction of dye chromophore structures) is preceded by the generation of a carbon-centered radical. Consistent with this, degradation of VBR must occur via three different pathways (two oxidative degradations and one *N*-de-alkylation) due to formation of different radicals (either a carbon-centered or nitrogen-centered radical). There is no doubt that the •OH attack on the dye yields a dye cationic radical. After this step, the cationic radical $Dye^{\bullet+}$ can undergo hydrolysis and/or use various deprotonation pathways, which in turn are determined by the different adsorption modes of VBR on the TiO_2 particle surface.

4. Conclusions

VBR dye can be successfully decolorized and degraded by TiO_2 under UV irradiation. Both *N*-de-alkylation and oxidative degradation of the VBR dye take place in the presence of TiO_2 particles. The reaction mechanisms of TiO_2/UV proposed in this study should shed some light on future application of the technology to the decolorization of dyes.

Acknowledgment

This research was supported by the National Science Council of the Republic of China.

References

[1] M.A. Fox, D.F. Duxbury, The photochemistry and photophysics of triphenylmethane dyes in solid and liquid media, Chem. Rev. 93 (1993) 381–433.
[2] Ullmann's Encyclopedia of Industrial Chemistry (UEIC), Triarylmethane and Diarylmethane Dyes, Part A27, 6th ed, Wiley-VCH, New York, 2001.
[3] D.M. Marmion, Handbook of U.S. Colorants, John Wiley & Sons, New York, 1991.
[4] M.S. Baptista, G.L. Indig, Effect of BSA binding on photophysical and photochemical properties of triarylmethane dyes, J. Phys. Chem. B 102 (1998) 4678–4688.
[5] C.R. Nelson, R.A. Hites, Aromatic amines in and near the Buffalo River, Environ. Sci. Technol. 14 (1982) 1147–1149.
[6] J.J. Black, M. Holmes, P.P. Dymerski, W.F. Zapisek, Fish tumor pathology and aromatic hydrocarbon pollution in a Great lakes estuary, in: B.K. Afghan, D. Mackoy (Eds.), Hydrocarbons and Halogenated Hydrocarbon in the Aquatic Environment, Plenum Press, New York, 1980, pp. 559–565.
[7] B.P. Cho, T. Yang, L.R. Blankenship, J.D. Moody, M. Churchwell, F.A. Bebland, S.C. Culp, Synthesis and characterization of *N*-demethylated metabolites of malachite green and leuco malachite green, Chem. Res. Toxicol. 16 (2003) 285–294.
[8] W. Azmi, R.K. Sani, U.C. Banerjee, Biodegradation of triphenylmethane dyes, Enzyme Microb. Technol. 22 (1998) 185–191.
[9] J.A. Bumpus, B.J. Brock, Biodegradation of crystal violet by the white rot fungus *Phanerochaete chrysosporium*, Appl. Environ. Microbiol. 54 (1988) 1143–1150.
[10] D.R. Doerge, M.I. Churchwell, T.A. Gehring, Y.M. Pu, S.M. Plakas, Analysis of malachite green and metabolites in fish using liquid chromatography atmospheric pressure chemical ionization mass spectrometry, Rapid Commun. Mass Spectrom. 12 (1998) 1625–1634.
[11] B.P. Cho, T. Yang, L.R. Blankenship, J.D. Moody, M. Churchwell, F.A. Bebland, S.J. Culp, Synthesis and characterization of *N*-de-methylated metabolites of malachite green and leucomalachite green, Chem. Res. Toxicol. 16 (2003) 285–294.
[12] S.J. Culp, P.W. Mellick, R.W. Trotter, K.J. Greenlees, R.L. Kodell, F.A. Beland, Carcinogenicity of malachite green chloride and leucomalachite green in B6C3F1 mice and F344 rats, Food Chem. Toxicol. 44 (2006) 1204–1212.
[13] B.P. Cho, L.R. Blankenship, J.D. Moody, D.R. Doerge, F.A. Beland, S.J. Culp, Synthesis and characterization of 4′-amino and 4′-nitro derivatives of 4-*N*,*N*-dimethylaminotriphenylmethane as precursors for a proximate malachite green metabolite, Tetrahedron 56 (2000) 7379–7388.
[14] L.M. Lewis, G.L. Indig, Effect of dye aggregation on triarylmethane-mediated photoinduced damage of hexokinase and DNA, J. Photochem. Photobiol. B 67 (2002) 139–148.
[15] H. Kyung, J. Lee, W. Choi, Simultaneous and synergistic conversion of dyes and heavy metal ions in aqueous TiO_2 suspensions under visible-light illumination, Environ. Sci. Technol. 39 (2005) 2376–2382.
[16] N. Watanabe, S. Horikoshi, A. Kawasaki, H. Hidaka, N. Serpone, Formation of refractory ring-expanded triazine intermediates during the photocatalyzed mineralization of the endocrine disruptor amitrole and related triazole derivatives at UV-irradiated TiO_2/H_2O interfaces, Environ. Sci. Technol. 39 (2005) 2316–2320.
[17] C.C. Chen, C.S. Lu, Y.C. Chung, Photocatalytic degradation of Ethyl Violet in aqueous solution mediated by TiO_2 suspensions, J. Photochem. Photobiol. A: Chem. 181 (2006) 120–125.
[18] A.L. Linsebigler, G.Q. Lu, J.T. Yates, Photocatalysis on TiO_2 surfaces: principles, mechanisms, and selected results, Chem. Rev. 95 (1995) 735–758.
[19] M.R. Hoffman, S.T. Martin, W. Choi, W. Bahnemann, Environmental applications of semiconductor photocatalysis, Chem. Rev. 95 (1995) 69–96.
[20] I.K. Konstantinou, T.A. Albanis, TiO_2-assisted photocatalytic degradation of azo dyes in aqueous solution: kinetic and mechanistic investigations: a review, Appl. Catal. B: Environ. 49 (2004) 1–14.
[21] Y. Murakami, E. Kenji, A.Y. Nosaka, Y. Nosaka, Direct detection of radicals diffused to the gas phase from the UV-irradiated photocatalytic TiO_2 surfaces by means of laser-induced fluorescence spectroscopy, J. Phys. Chem. B 110 (2006) 16808–16811.
[22] A.Y. Nosaka, J. Nishino, T. Fujiwara, T. Ikegami, H. Yagi, H. Akutsu, Y. Nosaka, Effects of thermal treatments on the recovery of adsorbed water and photocatalytic activities of TiO_2 photocatalytic systems, J. Phys. Chem. B 110 (2006) 8380–8385.
[23] G. Liu, X. Li, J. Zhao, H. Hidaka, N. Serpone, Photooxidation pathway of sulforhodamine-B. Dependence on the adsorption mode on TiO_2 exposed to visible light radiation, Environ. Sci. Technol. 34 (2000) 3982–3990.
[24] J.C. Zhao, T. Wu, K. Wu, K. Oikawa, H. Hidaka, N. Serpone, Photoassisted degradation of dye pollutants. 3. Degradation of the cationic dye rhodamine B in aqueous anionic surfactant/TiO_2 dispersions under visible light irradiation: evidence for the need of substrate adsorption on TiO_2 particles, Environ. Sci. Technol. 32 (1998) 2394–2400.
[25] C.C. Chen, H.J. Fan, C.S. Lu, C.Y. Jang, J.L. Jan, H.D. Lin, Photooxidative *N*-demethylation of crystal violet dye in aqueous nano-TiO_2 dispersions under visible light irradiation, J. Photochem. Photobiol. A: Chem. 184 (2006) 147–154.
[26] J.C. Zhao, H. Hidaka, A. Takamura, E. Pelizzetti, N. Serpone, Photodegradation of surfactants. 11. zeta.-Potential measurements in the photocatalytic oxidation of surfactants in aqueous titania dispersions, Langmuir 9 (1993) 1646–1650.
[27] C.C. Chen, C.S. Lu, Mechanistic studies of the photocatalytic degradation of methyl green: an investigation of products of the decomposition processes, Environ. Sci. Technol. 41 (2007) 4389–4396.
[28] X. Li, G. Liu, J. Zhao, Two competitive primary processes in the photodegradation of cationic triarylmethane dyes under visible irradiation in TiO_2 dispersions, New J. Chem. 23 (1999) 1193–1196.
[29] M. Saquib, M. Muneer, TiO_2-mediated photocatalytic degradation of a triphenylmethane dye (gentian violet), in aqueous suspensions, Dyes Pigments 56 (2003) 37–49.
[30] C.C. Chen, C.S. Lu, Photocatalytic degradation of Basic Violet 4: degradation efficiency, product distribution, and mechanisms, J. Phys. Chem. C 111 (2007) 13922–13932.
[31] J. Lee, W. Choi, Effect of platinum deposits on TiO_2 on the anoxic photocatalytic degradation pathways of alkylamines in water: dealkylation and *N*-alkylation, Environ. Sci. Technol. 38 (2004) 4026–4033.
[32] F.C. Shaefer, W.D. Zimmermann, Dye-sensitized photochemical autoxidation of aliphatic amines in non-aqueous media, J. Org. Chem. 35 (1970) 2165–2174.
[33] G. Galliani, B. Rindone, C. Scolastico, Selective de-methylation in the oxidation of arylalkylmethylamines with metal acetates, Tetrahedron Lett. 16 (1975) 1285–1288.